Optoacoustic real-time dosimetry for selective retina treatment

Georg Schuele
Medical Laser Center
Lübeck, Germany

Hanno Elsner
University of Lübeck
Department of Ophthalmology
Lübeck, Germany

Carsten Framme
Medical Laser Center
Lübeck, Germany
and
University of Regensburg
Department of Ophthalmology
Germany

Johann Roider
University of Kiel
Department of Ophthalmology
Germany

Reginald Birngruber
Ralf Brinkmann
Medical Laser Center
Lübeck, Germany

Abstract. The selective retina treatment (SRT) targets retinal diseases associated with disorders in the retinal pigment epithelium (RPE). Due to the ophthalmoscopic invisibility of the laser-induced RPE effects, we investigate a noninvasive optoacoustic real-time dosimetry system. *In vitro* porcine RPE is irradiated with a Nd:YLF laser (527 nm, 1.7-μs pulse duration, 5 to 40 μJ, 30 pulses, 100-Hz repetition rate). Generated acoustic transients are measured with a piezoelectric transducer. During 27 patient treatments, the acoustic transients are measured with a transducer embedded in an ophthalmic contact lens. After treatment, RPE damage is visualized by fluorescein angiographic leakage. Below the RPE damage threshold, the optoacoustic transients show no pulse-to-pulse fluctuations within a laser pulse train. Above threshold, fluctuations of the individual transients among each other are observed. If optoacoustic pulse-to-pulse fluctuations are present, RPE leakage is observed in fluorescein angiography. In 96% of the irradiated areas, RPE leakage correlated with the optoacoustic defined threshold value. A noninvasive optoacoustic real-time dosimetry for SRT is developed and proved *in vitro* and during patient treatment. It detects the ophthalmoscopically invisible laser-induced damage of RPE cells and overcomes practical limitations of SRT for use in private practice.
[DOI: 10.1117/1.2136327]

Keywords: selective retina treatment; optoacoustic dosimetry; real-time dosimetry; laser; retina.

Paper 04242R received Dec. 8, 2004; revised manuscript received May 25, 2005; accepted for publication Jun. 8, 2005; published online Dec. 8, 2005. This paper is a revision of a paper presented at the SPIE conference on Ophthalmic Technologies XIV, Jan. 2004, San Jose, CA. The paper presented there appears (unrefereed) in SPIE Proceedings Vol. 5314.

1 Introduction

The first use of lasers in medicine was for the treatment of retinal diseases. Due to the optical transparency of the eye, laser energy can be effectively delivered to the retina. Continuous wave (cw) photocoagulation became the gold standard treatment for several retinal diseases.[1–3] Photocoagulation of the retina with a cw laser (50 to 300-ms exposure time) results in visible laser burns of the retina, causing immediate functional loss in the treated area, a so-called scotoma. Novel retinal treatment modalities try to induce a specific therapeutic effect, but avoid damage of the photoreceptors and neural retina by selective targeting of different fundus structures. The mechanisms behind these techniques range from a photochemical effect in photodynamic therapy (PDT),[4] pure thermal in transpupillary thermotherapy (TTT),[5] to thermomechanical in selective retina treatment (SRT).[6–8] Due to the high inter- and also intra-individual variability of the optical transmission of the eye, blood perfusion of the choroidal vessels, and light absorption within the fundus, a real-time dosimetry method is preferable to ensure the selectivity and to monitor the therapeutic treatment progress.

In SRT, a train of microsecond laser pulses is applied to the retina.[6] Up to 60% of the incident light is absorbed by the melanosomes inside the retinal pigment epithelium (RPE) cells.[9] Since the exposure time is short compared to the thermal relaxation of the several micrometer thick RPE layer, the induced heat is confined to the RPE cell layer. This results in selective heating of the RPE cell layer. Calculations show that the induced temperatures at the adjacent photoreceptors are substantially lower than in the RPE.[10] It has been shown that applying a train of microsecond (μs) laser pulses destroys the RPE selectively, thus maintaining full vision in the treated area.[8] This technique allows treatment in proximity of the fovea.

SRT targets different diseases that are associated with decreased metabolic activity of the RPE. The aim of SRT is the rejuvenation of the RPE by inducing a RPE healing process. So far, more than 200 patients with diabetic maculopathy, central serous retinopathy, or drusen maculopathy were treated in a preclinical study. The rationale for treating these diseases with SRT is described next.

Diabetic maculopathy (DMP) is a disease of the mi-

Current affiliation: Lumenis, Inc., 2400 Condensa St., Santa Clara, CA 95051, E-mail: gschuele@lumenis.com

1083-3668/2005/10(6)/064022/11/$22.00 © 2005 SPIE

crovascular system caused by high sugar levels over a long period of time. The best predictor of diabetic retinopathy is the duration of the disease.[11] Patients who have had diabetic type 1 for more than 20 years show an incidence of 95% for DMP. In diabetic maculopathy, the altered microvascular system leads to localized or diffuse fluid accumulation within the retina, forming cystoid pockets of fluid in the outer plexiform layer in late stages of the disease. This retinal thickening leads to profound functional loss. The rational for treating DMP with lasers is to alter the RPE to increase metabolic activity and to thereby reduce retinal edema.[12] This would stabilize or even improve visual function. However, conventional argon laser treatment leads to irreversible photoreceptor damage and to microscotoma. Especially in cases with diabetic pathology close to the fovea, conventional argon laser treatment is no option. SRT treats the RPE while sparing retinal structures. Pathology close to the fovea can be tackled.

Central serous retinopathy (CSR) is a common retinal disorder characterized by an idiopathic serous neural retinal detachment in the macular region. Typically, CSR affects men aged 20 to 50 years. The typical CSR case shows a small leak on the level of the RPE, which can be identified easily by fluorescein angiography. Through this leak, serous fluid from the choroid detaches the retina. If the fovea is affected, the patient realizes functional loss, which is reversible if the duration of the retinal detachment is short. By applying only several laser spots to the RPE leakage site, the area is treated. However, 75% of the leaking sites are located within one disk area close to the fovea, so a conventional argon laser has substantial risk of damaging retinal tissue close to the fovea. SRT selectively closes the RPE leak and spares retinal tissue, and is therefore the only therapeutical option for treating the case with RPE leaks close to the fovea.

Age-related macular degeneration (AMD) is the leading cause of central visual loss among individuals 65 years of age and older in developed countries.[13–16] The disease primarily affects the choriocapillaris, Bruch's membrane, and RPE. The average age at onset of visual loss is about 75 years. In early stages, metabolic deposits (drusen) are localized between the RPE cells and Bruchs membrane, and are precursors of advanced AMD, either dry geographic or neovascular AMD. Drusen are a sign of collapsing metabolic transport from the RPE cells to the choroid occurring with age. The rational of treating drusen with SRT is to selectively damage RPE cells in the area of drusen to improve metabolic activity. This can reduce the amount and number of drusen material, and could positively influence the natural course of the disease and prevent development of late stage AMD.

In SRT, the selective RPE damage is ophthalmoscopically invisible but can be visualized invasively after treatment by fluorescein or indio-cyanine green (ICG) angiography.[6–8] This implies several limitations of this novel treatment for common use. First, treatment is only possible if also an angiography device is accessible. Second, the success of the laser treatment is only visible after an angiography. Third, angiography generally is an invasive technique (intravenous dye injection) with the risk of allergic reactions, anaphylactic shock, or death.

The formation of microbubbles around the strong absorbing melanosomes inside the RPE has proved to be the damage mechanism during irradiation of the RPE with μs laser pulses.[10,17] In this case, mechanical effects such as cell disruption from intracellular microbubbles most likely induce RPE cell damage. For laser pulses shorter than several nanoseconds, cell damage can also be induced by microbubbles or by stress waves.[18,19] For longer laser pulses (>500 μs), the RPE cells are assumed to be thermally denaturated.[20,21]

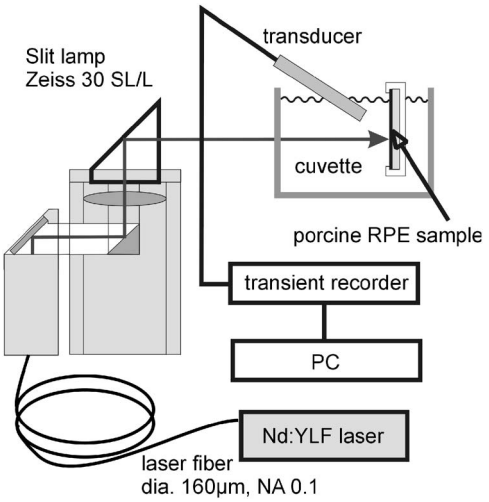

Fig. 1 Setup for optoacoustic measurements during irradiation of porcine RPE with μs-laser pulses.

If energy is absorbed and converted to heat, the thermoelastic expansion of the absorbing medium will generate an optoacoustic (OA) transient.[22,23] OA techniques have been used in ophthalmology to monitor the laser-induced retinal temperature increase *in vitro* during continuous wave (cw) photocoagulation and during SRT patient treatment.[24] Also, OA imaging of the ciliary body and OA monitoring of transscleral cyclophotocoagulation is possible *in vitro*.[25] In another *in vitro* study, OA techniques are used for temperature mapping of tissue during laser-induced thermotherapy (LITT).[26–28]

During irradiation of RPE with μs laser pulses, an OA transient will be produced.[24] Due to the formation and collapse of microbubbles around the melanosomes during a successful SRT, additional OA bubble transients will be emitted.[29] This is analogous to the emission of acoustic transients during formation and collapse of cavitation bubbles.[30]

The objective of this study was to develop and validate a real-time OA dosimetry system for SRT. This system should reliably detect the laser-induced microbubble formation around the melanosomes during a successful treatment of irradiation.

2 Material and Methods

2.1 *In Vitro Experiments*

2.1.1 *Setup for in vitro experiments*

An intracavity frequency-doubled, pulse-stretched Nd:YLF laser (527 nm, 1.7-μs pulse duration, 100-Hz repetition rate) was used as an irradiation source. A more detailed description of the laser itself can be found elsewhere.[10] The fiber tip was imaged with an ophthalmic laser slit lamp (Zeiss, 30 SL/L) to the sample, which was fixed in a water-filled cuvette (Fig. 1). The beam diameter and profile in the sample plane was mea-

sured with a laser beam analyzer (LBA-300PC, Spiricon Incorporated, Logan, UT). The beam profile was a tophat with an intensity variation of 15% due to speckle formation. The beam diameter was 160 μm in air. Acoustic transients were received with a commercial available ultrasonic broadband transducer (Valpey-Fisher, VP-1093, 0 to 10 MHz), preamplified (Panametrics, Model 5676, 54-dB amplification), and recorded by a transient recorder (TEK/Sony, RTD710). The distance between sample and transducer was approximately 2 mm. A hydrophone (Ceram number 118) generating 15 mV/bar was used to calibrate the broadband ultrasonic transducer, yielding a sensitivity of 1.05 V/bar at 1 MHz. For calibration, both detectors were placed in a water bath. They were adjusted to the same angle and the same distance to a black absorber sample. Laser pulses with 150 ns in duration and 20 to100-μJ pulse energy were applied to the sample, and the amplitude of the generated thermoelastic transient was measured simultaneously with an oscilloscope (TEK, TDS220).

2.1.2 *In vitro retinal pigment epithelium sample preparation, vitality staining, and laser parameters*

The experiments were performed on six freshly enucleated porcine eyes from the slaughterhouse. After equatorial dissection, the vitreous, neural, and neurosensory tissue, including the photoreceptors, were carefully removed. The sample with RPE as a superficial layer was fixed in a holder system and covered with physiological saline solution. After irradiation, the sample was stained with the vitality marker CalceinAM (Molecular Probes). Due to the uncharged structure of CalceinAM, it can penetrate the cell membrane. Once inside the cell, the lipophilic blocking groups (AM) are cleaved by nonspecific esterases, and Calcein is unblocked. The intracellular released Calcein fluoresces when excited with blue light at 480 nm.[31] Living cells fluoresce brightly due to the accumulated Calcein compared to dead cells without esterases, which appear dark in the fluorescence microscope image (Fig. 2).

For the *in vitro* experiments, we used the clinical treatment parameter with 30 laser pulses at a repetition rate of 100 Hz. Due to the lower damage threshold of *in vitro* porcine RPE,[10] between 5 to 35 μJ per pulse were applied to the samples.

2.2 *Patient Treatment*

2.2.1 *Setup for patient treatment*

We used the same laser/slitlamp system as described before. During treatment, a contact lens was placed on the patient's cornea to eliminate the corneal refraction and to fix the eye. We modified a standard contact lens (Haag-Streit Laser-Lens 903L) with a piezzo-electric transducer (Fig. 3). The ring-shaped transducer (lead zirconium titanate, PZT5) with a resonance frequency of 1 MHz was embedded into the contact lens and electromagnetically shielded by copper foil. The sensitivity of the OA contact lens was calibrated with a hydrophone (Ceram, number 118, 15 mV/bar) to 5.1 V/bar at 1 MHz. For calibration, both detectors were placed in a water bath. They were adjusted to the same angle and the same distance to a black absorber sample. Laser pulses with 150 ns in duration and 20 to 100-μJ pulse energy were applied to the sample, and the amplitude of the generated thermoelastic transient was measured simultaneously with an oscilloscope (TEK, TDS220).

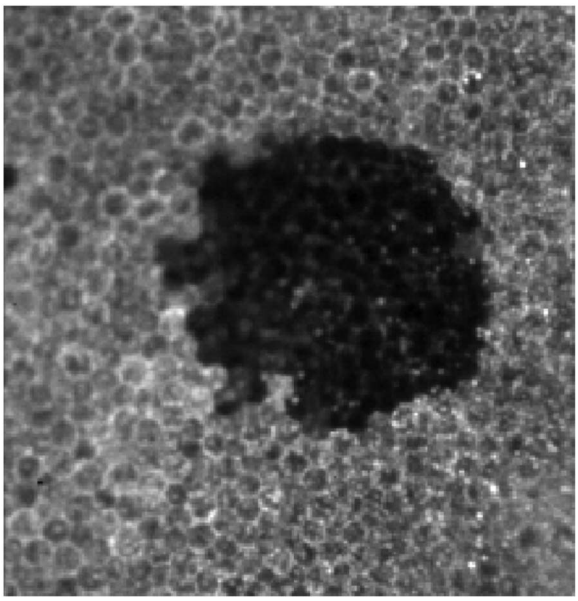

Fig. 2 CalceinAM stained porcine RPE cells. Live cells fluoresce while dead cells appear dark.

During treatment, the signals from the transducer were amplified (Panametrics, Model 5676, 40-dB amplification) and recorded by a data acquisition board (Datel, PCI 431-B, 10-MHz sample rate) in a personal computer (PC). The data acquisition process and the analysis were programmed with LabView (National Instruments 5.1). All treatments were recorded with a video system attached to the slitlamp to monitor the treatment and make the angiographic results comparable to the measured OA transients.

2.2.2 *Patient treatment parameters and proof of retinal pigment epithelium damage*

The OA data were taken during patient treatment in a clinical pilot study for SRT at the eye clinic of the Medical University Lübeck. All 27 patients gave written informed consent to treatment and measurement. The clinical treatment parameters for SRT were 30 laser pulses at a repetition rate of 100 Hz. Pulse energies ranged between 50 and 140 μJ. Due to a magnification factor of 1.1 of the contact lens, the retinal illumination diameter was 176 μm. Patients with diabetic maculopathy (DMP, 16 patients), central serous retinopathy (CSR, 5 patients), and drusen maculopathy (AMD, 6 patients) were treated. The number of laser lesions per treatment ranged from 10 up to 90 (mean 48) lesions per patient.

After treatments, fluorescein or indio-cyanine green (ICG) is intravenously injected. If RPE cells or their tight junctions are damaged, the outer blood-retina barrier is broken, and the dye can diffuse from the choriocapillaris to the retina. The damaged areas were visualized by fluorescein (FLA) or ICG angiography (Heidelberg Instruments, HRA).

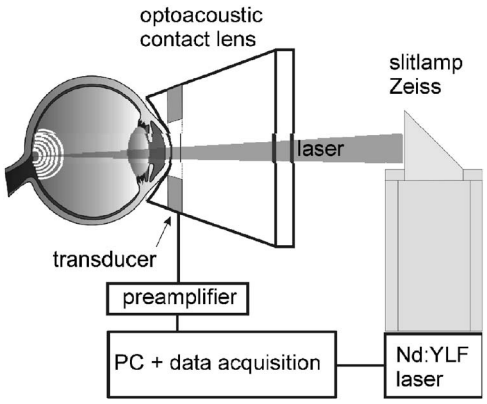

Fig. 3 Setup for optoacoustic measurements during patient treatment with μs-laser pulses.

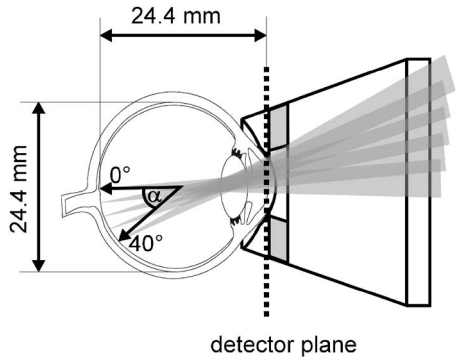

Fig. 4 Geometry for acoustic simulation of the OA contact lens. The simulated retinal treatment locations range from 0 to 40 deg.

2.3 *Acoustic Detection Simulation of the Optoacoustic Contact Lens*

Due to the different treatment locations within the eye, the OA transients reach the piezo-electric transducer from different angles. This leads to strong distortions of the detected transients. The surgeon also tilts the contact lens during treatment to avoid dazzle of the illumination light reflection on the contact lens surface and to aim to different treatment locations. An adjustment to the acoustic axis of every treatment location during treatment is impractical; therefore, we studied the effect of acoustic transient distortion due to alteration of the acoustic path.

The effect on OA transient distortion due to different retinal treatment locations was examined by the use of an acoustic field simulation. The geometric assumptions of the simulations are shown in Fig. 4. The software package ULTRASIM[32] (programmed under MatLab at University of Oslo) was used. It simulates the acoustic field of various geometries under the Huygens principle, and was designed for optimization of medical ultrasonic transducers. A single $\sin^2$-shaped 1-μs-long acoustic wave is emitted from 20 point sources within the 160-μm illumination diameter at different locations within the eye, as shown in Fig. 4. The pressure distribution within the detector plane is calculated for different time points. A numerical integration over the ring-shaped detector structure within the detector plane leads to the calculated transients.

2.4 *Optoacoustic Data Analysis*

Although the measured OA transients showed a significant difference in pulse-to-pulse reproducibility for damaged and nondamaged RPE cells, the extraction of a reliable measure of this effect was not possible just by analyzing the frequency spectra or the acoustic power of the signals. The main problem was that, especially during patient treatment, the acoustic transfer function changed from treatment spot to treatment spot, and thus also the form and amplitude of the OA transients. Also, the subtraction of a thermoelastic reference transient is inappropriate. To overcome these problems, we developed an algorithm that takes these variabilities into account. The algorithm analyzes the OA transients in real time, and allows a determination if RPE cells are damaged or not.

In the first step, the mean transient $\bar{P}(t)$ of the 30 OA transients $P_j(t)$ per irradiation area is calculated.

$$\bar{P}(t) = \frac{1}{n}\sum_{j=1}^{n} P_j(t). \tag{1}$$

Second, the mean transient $\bar{P}(t)$ is subtracted from every single transient $P_j(t)$ to get 30 deviation transients $D_j(t)$.

$$D_j(t) = P_j(t) - \bar{P}(t). \tag{2}$$

After temporal integration in the time window t_1 and t_2 of the absolute value of the deviation transients $D_j(t)$, we extract the maximum of the $n=30$ integral values.

$$OA-\text{value} = \max\left[\int_{t_1}^{t_2} |D_j(t)|dt\right]: j = 1 \ldots n. \tag{3}$$

This value, called the OA value, gives a measure of the maximum pressure difference between the OA transients within a pulse train.

Due to a lack of a thermoelastic reference transient during treatment, the mean transient $\bar{P}(t)$ from Eq. (1) is used. By subtraction from the measured transients $P_j(t)$, the thermoelastic parts are removed, as these are stable within one treatment spot. In the case of a subthreshold lesion, one extracts only the electrical and acoustic noise of the measurement. In a successful irradiation, microbubbles are generated. In this case, Eq. (2) extracts only the microbubble-induced acoustic transients, which are randomly formed. By choosing the maximum value [Eq. (3)] of the deviation transients $D_j(t)$, the detection of a single microbubble formation is ensured.

3 Results

3.1 *Detection Characteristic of the Optoacoustic Contact Lens*

With respect to different retinal target points, the expansion of the OA transient was simulated as described in Sec. 2.3. The pressure distribution within the detector plane was calculated for different times after laser impact on the retinal location. Figure 5 shows a typical series of pressure distributions in the detector plane for a 10-deg tilt off the central spot. The de-

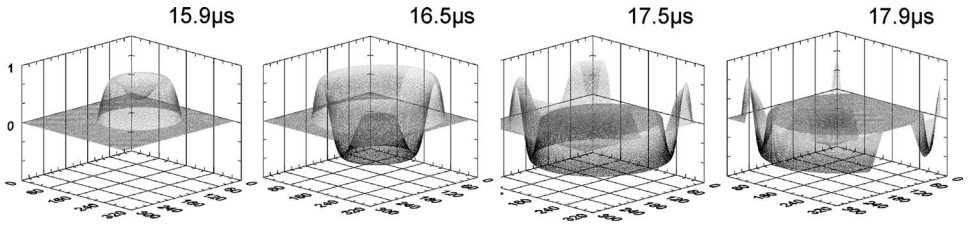

Fig. 5 Pressure distribution in the detector plane at different times for a 10-deg tilt of the target point in the eye. The decentral appearance of the pressure wave is clearly visible. For each temporal point, the numerical integration of the pressure values over the detector area leads to the pressure amplitude.

central appearance of the pressure wave is clearly visible. For each temporal point, the numerical integration of the pressure values over the detector area leads to the pressure amplitude.

The simulated OA transients for the tilting range from 0 to 40 deg are shown in Fig. 6. During SRT, 0 deg refers to a location slightly above the fovea, and 40 deg will be outside of the retinal arcade vessels. The 0-deg transient shows the highest amplitude and shortest bipolar transient. Even in this case, the emitted $\sin^2$ burst is strongly distorted and stretched by a factor of 1.5, owing to the ring detector geometry. For higher tilt angles, the amplitude is lowered up to a factor of 2, and the transient is strongly distorted and stretched up to a factor of 5. This is due to the longer transmission time of the pressure wave over the detector area. The emitted mean frequency of 1 MHz from the retinal target location is shifted to lower frequencies, down to 0.6 MHz, while higher frequency components are strongly rejected.

With respect to these simulations, the variability of the expected amplitude, shape, and frequencies of the OA transient during SRT is expected to be high. Based on this simulation, the data analysis method described in Sec. 2.4 does not rely on a fixed OA transient shape.

3.2 *Optoacoustic Transients and Optoacoustic Retinal Pigment Epithelium Damage Detection In Vitro on Porcine Retinal Pigment Epithelium Samples*

A typical set of different OA transients recorded during irradiation of RPE samples is shown in Fig. 7. All graphs show a

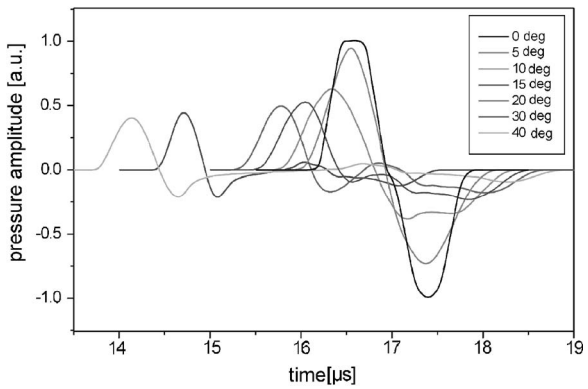

Fig. 6 Simulated pressure transients according to the geometric tilt of the retinal target area. Depending on the tilting angle, the pressure transients are temporally stretched, showing different amplitudes and different temporal onsets.

superposition of the 30 OA transients of a pulse train of different areas within one sample. At an exposure of 100 mJ/cm^2, which is below the RPE damage threshold, 30 pure thermoelastic OA transients are measured [Fig. 7(a)]. As the distance of the acoustic detector to the sample was 2 mm, the measurement was in the acoustic far field of the acoustic source (160-μm spot). For this reason, the OA transient is bipolar, followed by acoustic reflections within the detector. The 30 OA transients differ only by the noise level of the detection system. The measured pressure amplitude was 0.75 mbar. Slightly above the RPE damage threshold [Fig. 7(b)], the bipolar parts of the 30 OA transients remained unchanged. Only at the end of the bipolar part, small pulse-to-pulse fluctuations with 100-μbar amplitude are detectable. Increasing the exposure 25% above the RPE damage threshold [Fig. 7(c)], we found that the OA pulse-to-pulse fluctuations were strongly increased and nearly as big as the thermoelastic part of the OA transients. Also, the temporal onset of the fluctuations is earlier compared to the lower exposures seen in Fig. 7(b). At 2.5 times the threshold exposure, the amplitudes of the fluctuations strongly overwhelmed the thermoelastic transient [Fig. 7(d)]. A second bipolar transient is generated after several microseconds. The delay between the first and the second bipolar peak is reduced for each of the following laser pulses.

All measured OA transients were analyzed as described in Sec. 2.4. In Fig. 8, the OA value is plotted over the percentage of dead RPE cells within the illumination spot. The OA threshold value $OA_{vitro}=2.4\times10^{-10}$ (bar·s) was determined by minimizing the number of false positive and false negative results. This value was now used to differentiate between damaging and nondamaging irradiations. It is therefore possible to detect a microbubble formation signal of several cells under the thermoelastic OA transients of 80 cells within the illumination area. Of the 142 illuminations of five RPE samples, only three were false positive and three false negative. The RPE damage threshold values were recalculated into their single dichotome values (0=dead, 1=live) and analyzed with a Probit algorithm[33,34] (SPSS, Chicago IL). The damage threshold of porcine RPE cells was found to be $ED_{50}^{RPE}=194$ mJ/cm^2 with $ED_{85}^{RPE}=251$ mJ/cm^2 and $ED_{15}^{RPE}=149$ mJ/cm^2 as upper and lower widths of the adjusted logarithmic normal distribution, respectively. Converting the measured OA values to dichotome values ($0:OA\leqslant OA_{vitro}$, $1:OA\geqslant OA_{vitro}$) and utilizing the Probit analysis, a threshold for microbubble formation of $ED_{50}^{OA}=92$ mJ/cm^2 ($ED_{15}^{OA}=66$ mJ/cm^2; $ED_{85}^{OA}=128$ mJ/cm^2) was determined.

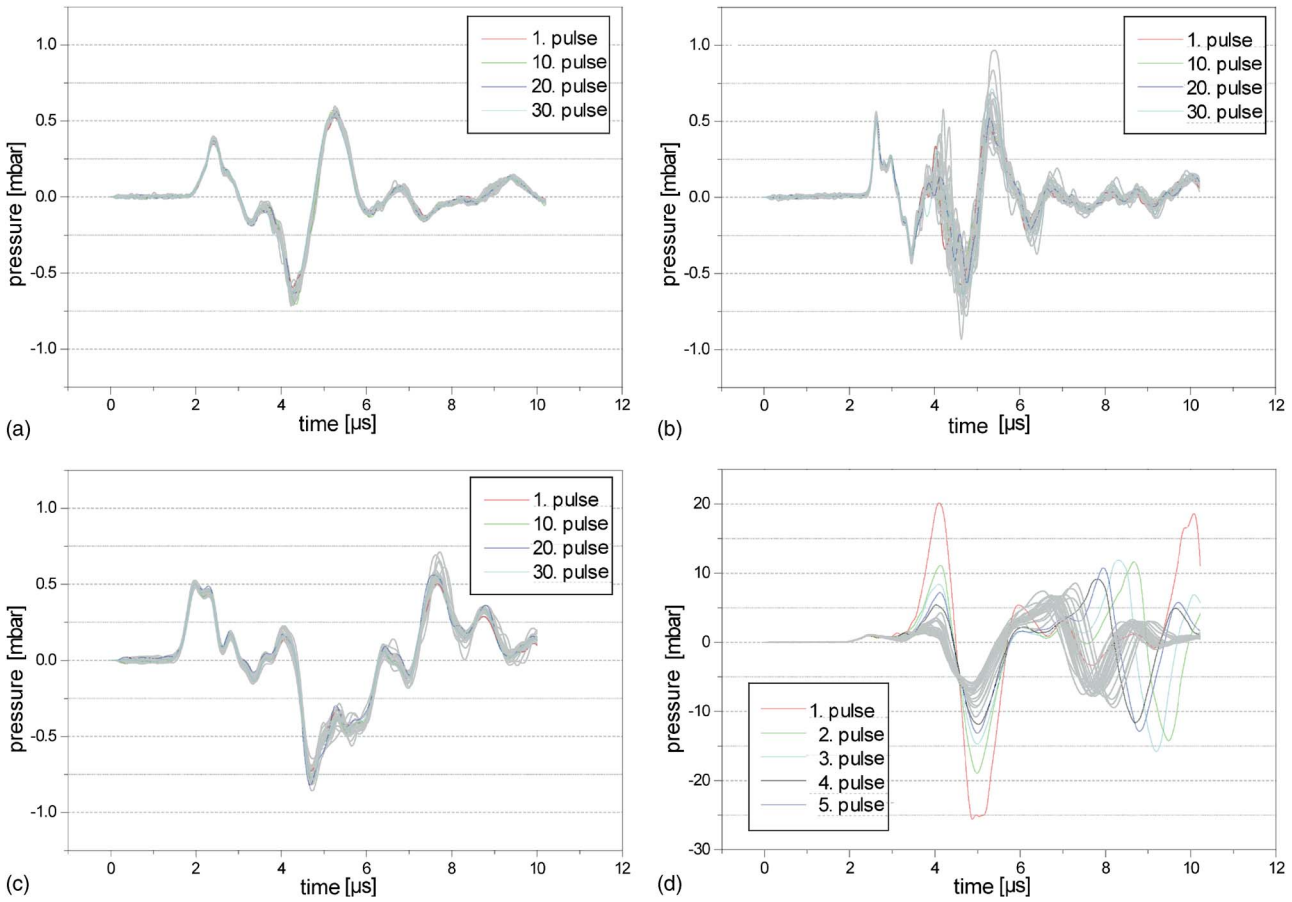

Fig. 7 30 superimposed OA transients during irradiation of fresh porcine RPE. (a) Below RPE damage (100 mJ/cm^2): only pure thermoelastic OA transients are observed, no pulse-to-pulse fluctuation. (b) Several damaged cells within the illuminated area (125 mJ/cm^2): thermoelastic OA transient with small pulse-to-pulse fluctuations are seen. (c) 25% above the damage threshold (150 mJ/cm^2): thermoelastic OA transients with strong pulse-to-pulse fluctuations and similar amplitudes are observed. (d) 250% over damage threshold (450 mJ/cm^2): strong bubble formation transients are observed with the formation of a second bipolar bubble collapse transient; these are much higher pressure amplitudes compared with the pure thermoelastic transients.

3.3 *Results During Selective Retina Treatment*

During 27 patient (27 eyes) SRT treatments, the OA transients were recorded. Overall, 1370 lesions were placed.

3.3.1 *Optoacoustic transient during SRT patient treatment*

All lesions placed in this study were ophthalmoscopically invisible. Due to the high sensitivity of 5.1 V/bar of the OA contact lens, it was possible to measure the generated OA transients during SRT. Two typical OA transients are shown in Fig. 9 for an angiographic visible lesion. Three different areas of interest are marked. After an acoustic transmission time of 5 μs, which corresponds to a geometric distance of 7.4 mm, a thermoelastic transient is detected [Fig. 9(a)]. This part of the transient was only generated in patients with turbid eye structures. Pulse-to-pulse fluctuations were never observed within this time window (5 to 13 μs). This signal was never measured for the young patient group (average age 40 years) with CSR (compare Fig. 10), which had clear eye structures. The measured acoustic distance of 7.4 mm of this OA transient generating structure relative to the OA contact lens corresponds to the distance of the anterior eye structures, i.e., the strong light absorbing iris where these signals are generated by the absorption of scattered light. After approximately 14 μs, a thermoelastic bipolar transient was measured [Fig. 9(b)]. The acoustic delay time corresponded to a distance of 21 mm (at 1532 m/s for vitreous body), which agrees with the distance of the transducer to the retina. This part in the time window between 14 and 22 μs was found in all OA transients measured during SRT. If pulse-to-pulse fluctuations are detectable, their onset is within this time window. The bipolar peak was followed by acoustic reflections within the OA contact lens, and oscillation of only a slightly damped resonant transducer with its resonant frequency of 1 MHz [Fig. 9(c)] was observed.

Comparing OA transients of patients below and above angiographic visible lesions shows similar transients as in the *in vitro* experiments on porcine RPE samples. Three typical superpositions of the 30 OA transients at different energies and locations within one patient eye (CSR, age 28 years) are shown in Fig. 10. For exposures that result in no angiographic visible lesions (50 μJ), the 30 OA transients showed no pulse-to-pulse fluctuations [Fig. 10(a)], and a pure thermoelastic transient is measured. The measured pressure am-

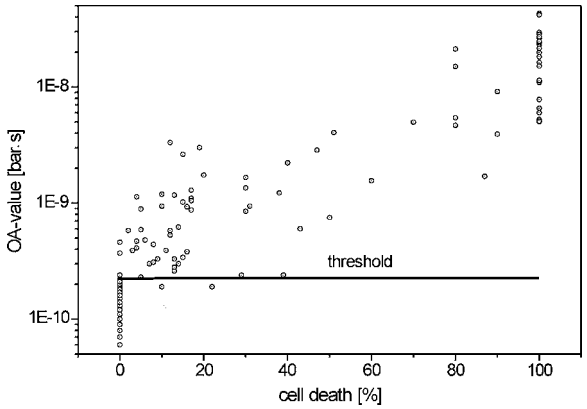

Fig. 8 OA value versus percent RPE cell death of six samples of six different eyes *in vitro*. Over all, 142 areas were illuminated. The threshold for optoacoustically detected RPE cell damage was determined as $OA_{vitro}=2.4\times10^{-10}$[bar·s] by minimizing the number of false-positive and false-negative results. In this case, only three locations were sorted as false positives and three as false negatives. The three false-negative results were still below the threshold for 50% cell death (ED50).

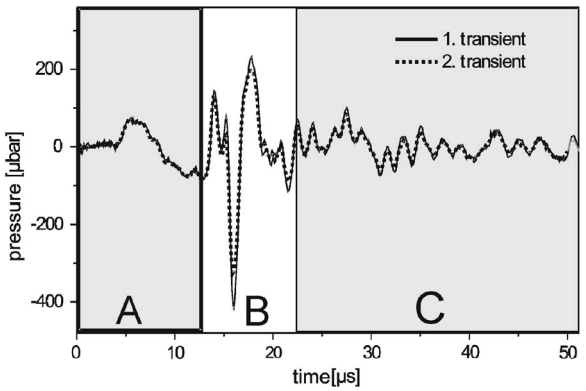

Fig. 9 Typical OA transients measured during SRT by use of the OA contact lens. Three different areas of interest are marked. (a) Thermoelastic transient induced by the anterior eye structure (iris) by scattered light from turbid eye media (was only detectable in patients with turbid media). (b) Thermoelastic transient of the RPE with pulse-to-pulse fluctuations. (c) Acoustic reflections within the OA contact lens and oscillation of the resonant transducer with its resonant frequency of 1 MHz.

plitudes are around 0.3 mbar. At higher exposure [Fig. 10(b), 125 μJ, angiographically visible], a strong thermoelastic bipolar transient is measured. However, small pulse-to-pulse fluctuations start within the bipolar peak. For the same exposure, but a different location within the eye, strong fluctuations and even a second bipolar peak is detectable for the first applied laser pulse [Fig. 10(c)]. This second bipolar peak was detected very rarely. In the over 1370 treatment spots that were applied during the 27 patient treatments, this second bipolar peak was detected only in three spots.

3.3.2 *Optoacoustic online dosimetry during patient treatment*

Roider et al.[6–8] introduced the fluorescein leakage observed in angiography as a reference standard for the detection of the ophthalmoscopic invisible selective RPE damage. With respect to our OA-based RPE damage detection, the OA values of every single spot were compared to the angiographic responses. A direct comparison of every single treatment spot was not possible in patients with DMP. The fundus of these patients shows a disease-related diffuse FLA leakage that makes it impossible to detect the additional laser-induced FLA spots. A direct correlation of treated laser spots succeeded only in the small group of four CSR patients. Nearly every single treatment lesion could directly be compared to the FLA result.

As the OA transients during patient treatment showed similar characteristics in comparison to the *in vitro* data, the same analysis algorithm was used. This analysis was limited to a temporal window from $t_1=12$ μs to $t_2=30$ μs, where most of the fluctuations appeared. To reduce the electromagnetic noise, the OA transients were filtered digitally with a fourth-order Butterworth filter (LabView) between 5 kHz and 1 MHz.

In Fig. 11, all analyzed OA values of these four treatments are plotted with respect to the pulse energy. The open symbols mark all angiographic visible lesions, filled gray symbols are the FLA negative, and the filled black symbols are the data points that were not analyzable due to multiple lesions being placed on the same spot. The Probit algorithm[33,34] was used to determine the OA threshold value *in vivo* as $OA_{vivo}=1.96\times10^{-10}$[bar·s]. In these four treatments, two out of 94 lesions were detected as false positives and two as false negatives. The OA threshold for an angiographic lesion during patient treatment of $OA_{vivo}=1.96\times10^{-10}$[bar·s] was found to be close to the threshold for porcine RPE damage, $OA_{vitro}=2.4\times10^{-10}$[bar·s].

As seen in Fig. 11, the OA values vary a lot within one eye at the same applied energy. In patients with DMP, lower OA values were generally achieved in edematous retinal locations.

3.3.3 *Optoacoustic value in comparison with indigo-cyanine green angiography intensity*

In the *in vitro* results of Fig. 8, it can be seen that as the OA values increased, more RPE cells were damaged within the treatment spot. During patient treatment, the amount of damaged RPE cells within a single spot was not accessible. During fluorescein angiography, the diffusion of fluorescein through the damaged RPE areas was too fast to get a measurement of the leakage size. The clearest FLA images are always seen in the early phase, several seconds after dye injection. In contrast to this, ICG diffuses very slowly through the damaged RPE areas. The best contrast for the visualization was in the very late phase, up to 20 min after injection. In ICG angiograms, the single treatment spots showed different fluorescence intensity [Fig. 12(a)]. Due to the nonlinearity of the whole ICG angiography process, the mean gray value of the spot gave a rough hint of the amount of damaged RPE cells within that spot.

The ICG angiogram image in Fig. 12(a) shows the location of each single lesion as a white circle. Within these circles, the mean gray value was analyzed for each associated lesion number. These mean gray values of the ICG angiogram are plotted with respect to the OA value for every corresponding

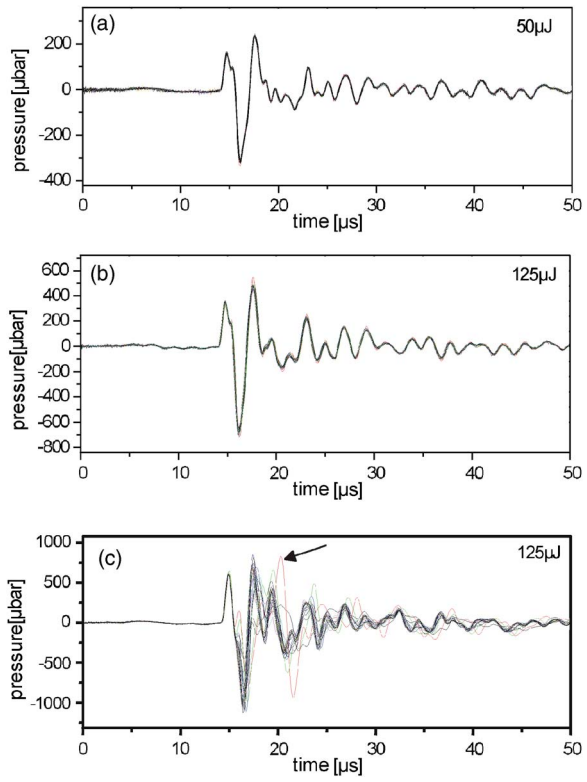

Fig. 10 Typical OA transients measured during patient treatment. (a) Subthreshold lesion at 50 μJ, angiographic invisible lesion, no pulse-to-pulse fluctuations. (b) Suprathreshold lesion at 125 μJ, angiographic visible lesion, small pulse-to-pulse fluctuations. (c) Suprathreshold lesion at 125 μJ, angiographic visible lesion, strong pulse-to-pulse fluctuations with bubble collapse sometimes detectable (arrow).

spot number [Fig. 12(b)]. It can be seen that the brighter the ICG spot, the higher the corresponding OA value. From this data, it appeared that during patient treatment, the OA dosimetry system detects the amount of damage applied to the RPE cells.

3.3.4 *Optoacoustic classification of 27 SRTs*

Overall, the OA dosimetry system was used during 27 SRT patient treatments. In the first stage of this study, test lesions at various laser pulse energies were applied to the fundus around the retinal vessel arcades. Based on the immediate fluorescein angiography results, the treatment in the central region was performed with laser pulse energies that showed successful FLA leakage in the test lesions. As the measured OA values during central treatment were far higher than the test lesions, the treatment energy was lowered according to the OA values obtained. Final FLAs after complete treatment indicated RPE damage in the central region at lower pulse energies, adjusted due to the OA value.

In the later phase of the study, the first FLA for the test lesion was canceled, and the treatment energy in the central area was only adjusted based on the OA values. In all cases, the FLA after laser treatment indicated successful damage of RPE, as noted by fluorescein leaking at the treatment spots.

To obtain an overview of the data for all 27 treatments, the results of the 1370 spots are summarized in Fig. 13. The measured OA values are sorted into three different categories.

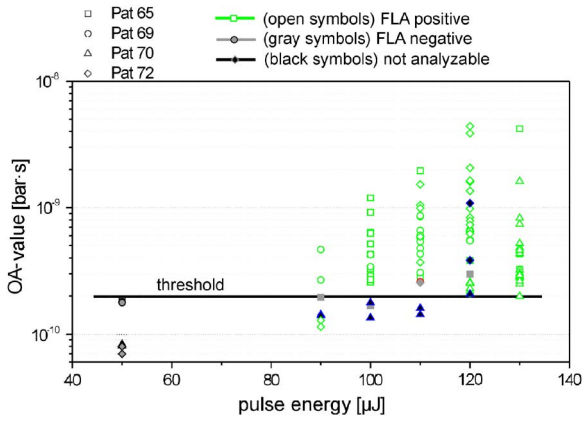

Fig. 11 OA value versus applied pulse energy for four patient treatments. The open symbols mark the FLA positive lesions, gray symbols mark the FLA negative, and the black symbols were not analyzable data points.

First, the range of OA values below the threshold of $OA_{vivo} = 1.96 \times 10^{-10}$[bar·s], with no pulse-to-pulse fluctuations and no RPE damage. Second, the therapeutic range of OA values are between 1.96×10^{-10}[bar·s] and 8×10^{-10}[bar·s], with angiographicly visible RPE damage and small pulse-to-pulse fluctuations. Finally, the range of OA values larger than 8×10^{-10}[bar·s] is grouped, with strong pulse-to-pulse fluctuations and occasionally detectable bubble collapse.

During the treatments, the laser pulse energy was adjusted so that the OA values were within the range of successful therapeutic treatment. This was difficult, even within one eye. On this basis, 23% of the lesions at 100-μJ pulse energies were overtreated, while 20% still did not show an adequate OA response. The variability of OA values over the therapeutic energy range from 80 to 150 μJ clearly demonstrates the necessity of a real-time dosimetry system during SRT.

4 Discussion

In this work, we introduced and proved the efficiency of an OA based real-time dosimetry system for SRT during *in vitro* and *in vivo* treatment.

4.1 *Detection of Optoacoustic Transients In Vivo and During Patient Treatment*

Due to the high sensitivity of the 1.05-V/bar ultrasonic transducer used for the *in vitro* experiments and the broadband preamplifier (54-dB amplification), we were able to reduce the noise level of the pressure amplitude down to 10 μbar at 1 MHz (Fig. 7). This high sensitivity enables the detection of thermoelastic transients during μs irradiation, which far exceeds the acoustic confinement time of the applied laser pulse, so that the pressure generation is less effective. As microbubble formation around the strong absorbing melanosomes inside the RPE cells was shown to be the primary RPE damage mechanism[10,17] for μs laser pulses, the onset of the detected pulse-to-pulse fluctuations of the OA transients [as seen in Fig. 7(b)] was consistent with the onset of damaged RPE cells within the exposed spot. These fluctuations can be linked to the acoustic formation and collapse transients during microbubble formation.[29] As the RPE cells contain several

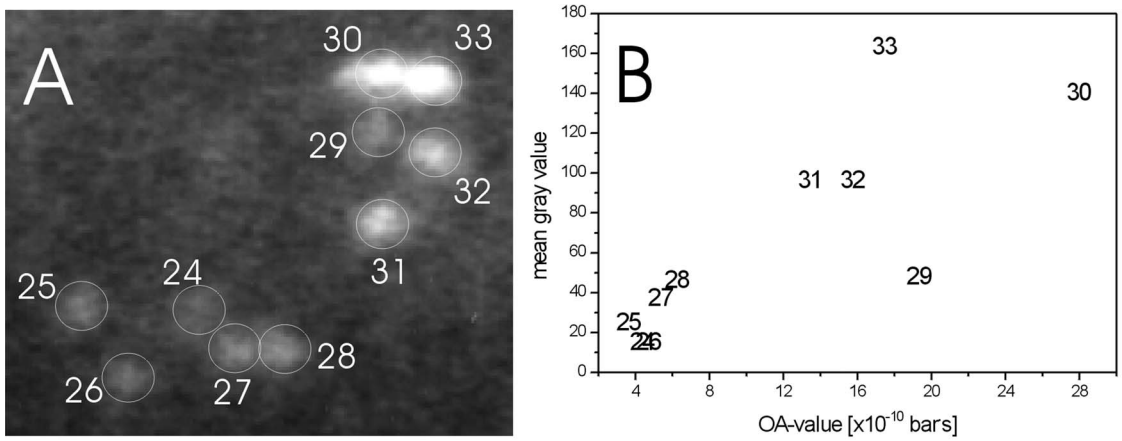

Fig. 12 (a) ICG angiography image with lesion locations (white circles) and the associated lesion number. (b) Analyzed OA values over mean gray value of the corresponding ICG spots. The brighter the ICG spot, the higher the measured OA values.

hundred melanosomes, and 80 RPE cells are illuminated within one spot, irregular microbubble formation is most probable. Also, early onset of the fluctuations by increasing the exposure [Figs. 7(b)–7(d)] can be explained by an earlier microbubble formation due to effective heating.[35] The second bipolar transients in Fig. 7(d) are most likely the collapse transients of big "macrobubbles," which were also detected by Kelly during threefold threshold exposures using nanosecond laser pulses.[19] The reduction of the delay time between the two following bipolar peaks can be induced by material ejection of the previous laser pulse. The OA detection system works well and reliably on porcine RPE samples. Even the damage of several cells within a spot of 80 illuminated cells can be detected. Therefore, the threshold ED_{50}^{OA} for microbubble formation is below the RPE damage threshold.

Due to the high sensitivity of 5.1 V/bar at 1 MHz of the OA contact lens, it was possible to detect the OA transients during patient treatment. The noise level could be reduced down to 2 μbar (Fig. 9). The OA transients measured during patient treatment coincided with the OA transients from experiments on porcine RPE samples. If RPE damage is detectable via an angiographic visible lesion in patients, then pulse-to-pulse fluctuations appear at the end of the thermoelastic bipolar peak [Fig. 10(b)]. Similar pulse-to-pulse fluctuations were detected if porcine RPE cells were damaged, as indicated by vitality staining with calceinAM. Also, in patient treatment, the fluctuations are linked to the microbubble formation around the melanosomes inside the RPE cells. This is further supported by the detection of a second bipolar peak [Fig. 10(c)], which can be identified as the bubble collapse transient.[30] In this case, the bubble lifetime was 6 μs.

The results of the simulation of the OA contact lens characteristics (Figs. 5 and 6) show that the acoustic transfer function strongly changes for different locations within the eye. During patient treatment, it was not possible to align the contact lens well at each treatment location, thus measurements of absolute pressure amplitudes and waveforms were not possible. This was taken into account by the analysis method used (Sec. 2.4). The method used the mean transient $\bar{P}(t)$ of all OA transients per pulse train as a reference, as the eye will not significantly move during the 300-ms exposure time. At every single spot, a new reference transient was defined and changes in the acoustic transfer function, for example due to movements, were eliminated. The developed analysis method is fast (30.2 ms on a Pentium 120 MHz), which makes it applicable for a real-time dosimetry system.

4.2 *Optoacoustic Dosimetry System Sensitivity*

Until now, selective RPE damage can only be detected by fluorescein or ICG angiography.[6–8,36] For this procedure, the dye is intravenously injected into the patient and visualized at the fundus with a fundus camera or laser scanning angiograph. Besides its invasive character, the main drawback of this monitoring technique is that it cannot be used as a real-time dosimetry method, which leads to practical limitations of SRT. For an ideal treatment, several steps are needed to insure a successful irradiation. First, test lesions at different energy levels are applied to the fundus around the retinal vessel arcades, and the first angiogram depicts the threshold energy. Second, the treatment is then performed with the determined threshold energy; however, a second angiogram is needed to confirm the induced lesions. In some cases, a second treatment is needed if the initially delivered treatment energy was too low. This invasive and time-consuming procedure is a practical limitation for SRT to become a standard treatment modality that can be performed in private practice. A real-time dosimetry method is highly desirable to bring this novel technique to broad application.

Our *in vitro* results show that the OA detection method is sensitive enough to detect only several damaged RPE cells within an exposed spot of 80 cells. An acoustically detected damage threshold can be detected at $OA_{vitro} = 2.4 \times 10^{-10}$ (bar·s) (Fig. 8). Due to the high acoustic detection sensitivity, the RPE damage threshold value of $ED_{50}^{RPE} = 194$ mJ/cm^2 (50% RPE damage) is higher than the threshold for microbubble formation $ED_{50}^{OA} = 92$ mJ/cm^2 (50% occurrence of microbubble formation within the spot). This also indicates that microbubble formation can be clearly detected if less than 50% of cells are damaged. In a more recent study,[17] we could also show that microbubble formation can even be detected if only one RPE cell is damaged. During patient treatment, an acoustic detected damage threshold can

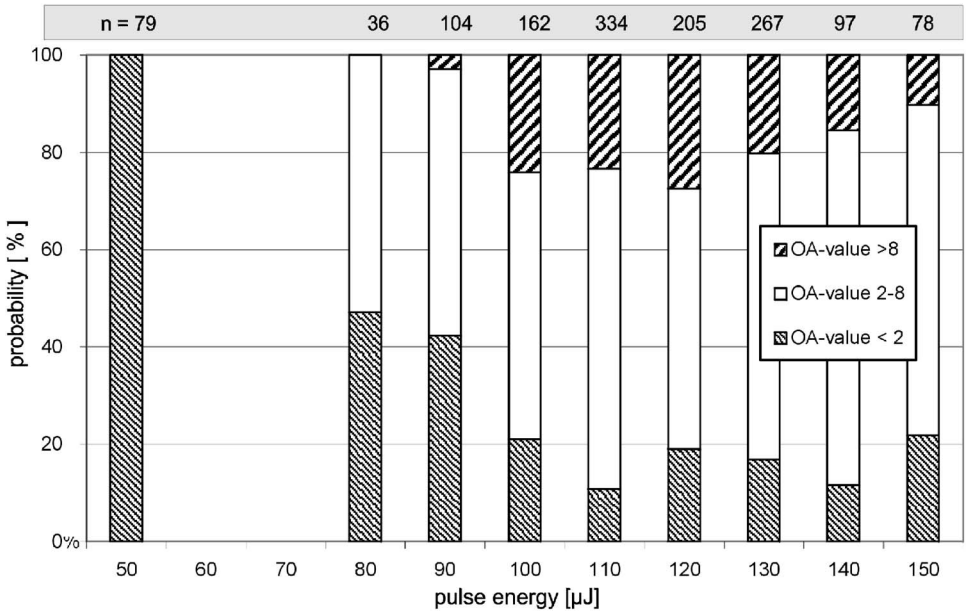

Fig. 13 Probability of three OA value ranges over pulse energies for 27 patient treatments (n=1370 lesions).

be defined as $OA_{vivo}=1.96\times10^{-10}$ (bar·s) (Fig. 11). This value is close to the threshold value for *in vitro* experiments (OA_{vitro}), which is surprising due to the different geometries of the transducers and acoustic transfer functions, which were not taken into account.

The results of the *in vitro* experiments (Fig. 8) also show that the higher the extracted OA value was, the more cells were damaged within one spot. The amount of damaged RPE cells cannot be directly analyzed in a patient. Therefore, as a very rough estimate, the gray level of an ICG angiography was correlated to the amplitude to the measured AO value. In Fig. 12(b) it can be seen that the brighter the ICG spot was, the higher the corresponding OA value. From this data, it seems that during patient treatment, the OA dosimetry system detects the amount of damaged RPE cells. However, a determination of the macroscopic damage was not possible. A better correlation of the detected OA value and the extent of RPE damage can only be done in direct comparison of single spots under histological examination, which is not possible in humans. Ultra-high-resolution optical coherence tomography (OCT) images,[37] which are applicable in humans, might allow further insight.

Due to the high variability in pulse energy that is needed to reach the acoustic threshold OA_{vivo} during patient treatments (Fig. 13), it appeared that an active control of the laser pulse energy would be reasonable. Especially in patients with diabethic maculopathy and hard drusen, the threshold energy was strongly varying, depending on the treatment location.

5 Conclusion

In this work, we introduce and prove the concept of an OA-based real-time dosimetry system for SRT. In porcine RPE samples *in vitro*, as well as in patient treatments, the OA dosimetry system detected the laser-induced RPE damage. More than 27 patient treatments are controlled by this system. The OA dosimetry system is embedded in a clinical SRT prototype laser and will be further evaluated during an ongoing clinical multicenter SRT study.

References

1. Macular Photocoagulation Study Group, "Laser photocoagulation of subfoveal recurrent neovascular lesions in age-related macular degeneration. Results of a randomized clinical trial.," *Arch. Ophthalmol. (Chicago)* **109**(9), 1232–1241 (1991).
2. Macular Photocoagulation Study Group, "Argon laser photocoagulation for senile macular degeneration. Results of a randomized clinical trial," *Arch. Ophthalmol. (Chicago)* **100**(6), 912–918 (1982).
3. The Diabetic Retinopathy Study Research Group, "Photocoagulation treatment of proliferative diabetic retinopathy: relationship of adverse treatment effects to retinopathy severity. Diabetic retinopathy study report no. 5," *Dev. Ophthalmol.* **2**, 248–261 (1981).
4. Treatment of Age-related Macular Degeneration with Photodynamic Therapy (TAP) Study Group, "Photodynamic therapy of subfoveal choroidal neovascularization in age-related macular degeneration with verteporfin: one-year results of 2 randomized clinical trials—TAP report.," *Arch. Ophthalmol. (Chicago)* **117**(10), 1329–1345 (1999).
5. M. A. Mainster and E. Reichel, "Transpupillary thermotherapy for age-related macular degeneration: long-pulse photocoagulation, apoptosis, and heat shock proteins," *Ophthalmic Surg. Lasers* **31**(5), 359–373 (2000).
6. J. Roider, R. Brinkmann, C. Wirbelauer, H. Laqua, and R. Birngruber, "Subthreshold (retinal pigment epithelium) photocoagulation in macular diseases: a pilot study," *Br. J. Ophthamol.* **84**(1), 40–47 (2000).
7. J. Roider, F. Hillenkamp, T. Flotte, and R. Birngruber, "Microphotocoagulation: Selective effects of repetitive short laser pulses," *Proc. Natl. Acad. Sci. U.S.A.* **90**, 8643–8647 (1993).
8. J. Roider, R. Brinkmann, C. Wirbelauer, H. Laqua, and R. Birngruber, "Retinal sparing by selective retinal pigment epithelial photocoagulation," *Arch. Ophthalmol. (Chicago)* **117**(8), 1028–1034 (1999).
9. B. R. Hammond and M. Caruso-Avery, "Macular pigment optical density in a southwestern sample," *Invest. Ophthalmol. Visual Sci.* **41**(6), 1492–1497 (2000).
10. R. Brinkmann, G. Huettmann, J. Rogener, J. Roider, R. Birngruber, and C. P. Lin, "Origin of retinal pigment epithelium cell damage by pulsed laser irradiance in the nanosecond to microsecond time regimen," *Lasers Surg. Med.* **27**(5), 451–464 (2000).
11. R. Klein, B. E. Klein, and S. E. Moss, "Epidemiology of proliferative diabetic retinopathy," *Diabetes Care* **15**(12), 1875–1891 (1992).

12. F. L. Ferris, "How effective are treatments for diabetic retinopathy?" *JAMA, J. Am. Med. Assoc.* **269**(10), 1290–1291 (1993).
13. J. D. Gass, *Stereoscopic Atlas of Macular Disease: Diagnosis and Treatment*, 4th ed., C. Mosby, Ed., Mosby, St Louis (1997).
14. H. M. Leibowitz, D. E. Krueger, L. R. Maunder, R. C. Milton, M. M. Kini, H. A. Kahn, R. J. Nickerson, J. Pool, T. L. Colton, J. P. Ganley, J. I. Loewenstein, and T. R. Dawber, "The Framingham eye study monograph: An ophthalmological and epidemiological study of cataract, glaucoma, diabetic retinopathy, macular degeneration, and visual acuity in a general population of 2631 adults, 1973–1975," *Surv. Ophthalmol.* **24**(suppl), 335–610 (1980).
15. R. Klein, B. E. Klein, S. C. Jensen, and S. M. Meuer, "The five-year incidence and progression of age-related maculopathy: the beaver dam eye study," *Ophthalmology* **104**(1), 7–21 (1997).
16. B. Rahmani, J. M. Tielsch, J. Katz, J. Gottsch, H. Quigley, J. Javitt, and A. Sommer, "The cause-specific prevalence of visual impairment in an urban population. The Baltimore eye survey," *Ophthalmology* **103**(11), 1721–1726 (1996).
17. G. Schuele, M. Rumohr, G. Huettmann, and R. Brinkmann, "RPE damage thresholds and mechanisms for laser exposure in the μs to ms time regimen," *Invest. Ophthalmol. Visual Sci.* **46**, 714–719 (2005).
18. C. P. Lin and M. W. Kelly, "Cavitation and emission around laser-heated microparticles," *Appl. Phys. Lett.* **72**(22), 1–3 (1998).
19. M. W. Kelly, "Intracellular cavitation as a mechanism of short-pulse laser injury to the retinal pigment epithelium," in *Electrical Engineering*, Tufts Univ. (1997).
20. R. Birngruber, "Thermal modelling in biological tissue," in *Lasers in Biology and Medicine*, R. P. F. Hillenkamp, Ed., pp. 77–97, Plenum, New York (1980).
21. R. Birngruber, F. Hillenkamp, and V. P. Gabel, "Theoretical investigations of laser thermal retinal injury," *Health Phys.* **48**(6), 781–796 (1985).
22. M. W. Sigrist and F. K. Kneubühl, "Laser-generated stress waves in liquids," *J. Acoust. Soc. Am.* **64**(6), 1652–1663 (1978).
23. M. W. Sigrist, "Laser generation of acoustic waves in liquids and gases," *J. Appl. Phys.* **60**(7), R83–R121 (1986).
24. G. Schuele, G. Huettmann, C. Framme, J. Roider, and R. Brinkmann, "Noninvasive optoacoustic temperature determination at the fundus of the eye during laser irradiation," *J. Biomed. Opt.* **9**(1), 173–179 (2004).
25. U. Oberheide, I. Bruder, H. Welling, W. Ertmer, and H. Lubatschowski, "Optoacoustic imaging for optimization of laser cyclophotocoagulation," *J. Biomed. Opt.* **8**(2), 281–287 (2003).
26. R. O. Esenaliev, I. V. Larina, K. V. Larin, and M. Motamedi, "Real-time optoacoustic monitoring during thermotherapy," *Proc. SPIE* **3916**, 302–310 (2000).
27. R. O. Esenaliev, A. A. Oraevsky, K. V. Larin, I. V. Larina, and M. Motamedi, "Real-time optoacoustic monitoring of temperature in tissues," *Proc. SPIE* **3601**, 268–275 (1999).
28. K. V. Larin, I. V. Larina, M. Motamedi, and R. O. Esenaliev, "Monitoring of temperature distribution in tissues with optoacoustic technique in real time," *Proc. SPIE* **3916**, 311–321 (2000).
29. G. Schuele, G. Huettmann, J. Roider, C. Wirbelauer, R. Birngruber, and R. Brinkmann, "Optoacoustic measurements during μs-s irradiation of the retinal pigment epithelium," *Proc. SPIE* **3914**, 230–236 (2000).
30. A. Vogel and S. Busch, "Schock wave emission and cavitation bubble generation by picosecond and nanosecond optical breakdown in water," *J. Acoust. Soc. Am.* **100**(1), 148–165 (1996).
31. Molecular Probes, "LIVE/DEAD viability/cytotoxicity," Product Information , Carlsbad, CA (2001).
32. S. Holm, F. Teigen, L. Odegaard, V. Berre, and J. O. Erstad, *ULTRASIM User's Manual*, Univ. of Oslo (1998).
33. SPSS, Technical Support, Probit (2001).
34. D. J. Finney, "Probit analysis: statistical treatment of the sigmoid response curve," Cambridge Univ. Press, London (1964).
35. J. Roegener, R. Brinkmann, and C. P. Lin, "Pump-probe detection of laser-induced microbubble formation in retinal pigment epithelium cells," *J. Biomed. Opt.* **9**(2), 367–371 (2004).
36. J. Roider, C. Lindemann, E. S. El-Hifnawi, H. Laqua, and R. Birngruber, "Therapeutic range of repetitive nanosecound laser exposures in selective RPE photocoagulation," *Graefe's Arch. Clin. Exp. Ophthalmol.* **236**, 213–219 (1998).
37. J. G. Fujimoto, "Optical coherence tomography for ultrahigh resolution *in vivo* imaging," *Nat. Biotechnol.* **21**(11), 1361–1367 (2003).